

Microscale-Patterned Graphene Electrodes for Organic Light-Emitting Devices by a Simple Patterning Strategy

Yang Chen, Nan Zhang, Yun-Fei Li, Yan-Gang Bi, Yuan-Yuan Yue, Jing Feng,*
and Hong-Bo Sun

Graphene grown by chemical vapor deposition has attracted much attention in optoelectronic application due to its great potential as a large-area 2D electrode material. However, the clean transfer and effective microscale patterning of graphene still remain great challenges for its use as the electrode in the optoelectronic devices. In this paper, a simple and reliable transfer-pattern strategy is developed for the microscale-patterned graphene electrode by using a photoresist as both supporting layer for the graphene transfer and photolithographic mask layer. The microscale-patterned graphene electrodes transferred onto the desired substrates exhibit low surface roughness of 0.675 nm and mean sheet resistance of $444 \Omega \square^{-1}$. 25 μm line width patterned organic light-emitting devices (OLEDs) arrays with high precision and uniform lighting area have proved the great potential of the transfer-pattern strategy for high-resolution OLEDs. Flexible and efficient OLEDs based on patterned graphene anodes can be realized by this strategy. Moreover, a scale of ≈ 2 in. patterned graphene well demonstrates the feasibility of the transfer-pattern strategy for large-area fabrication of the microscale-patterned graphene.

1. Introduction

As one of the most promising next-generation solid-state lighting and flexible display, organic light-emitting diodes (OLEDs) show remarkable performance, such as high efficiency, low power consumption, light weight, low cost, and mechanical flexibility.^[1–6] Transparent conductive electrode is an essential component for OLEDs which determines devices' performance through surface topography, light extraction, and charge transport. Up to now, indium-tin oxide (ITO) is still the broadly used electrode material in OLEDs because of its low resistance and high

transparency.^[7–10] However, the shortages of intrinsic sensitivity to acid and heat, the low storage of indium on earth, and intrinsic mechanical brittleness have impeded its application in OLEDs, especially flexible OLEDs. For the purpose to replace ITO electrodes, other transparent conductive materials such as metallic films,^[11–13] metal nanowires,^[14–16] conducting polymers,^[17–19] carbon nanotubes,^[20–23] and graphene^[24–27] have been widely investigated. Among them, 2D material of graphene is one of the most promising materials for a flexible transparent electrode because of its high transparency, excellent electrical conductivity, mechanical stability, and ultrahigh carrier mobility.^[28–33]

Microscale patterning of the graphene is a necessary and urgent demand for the use of the graphene as electrodes in the optoelectronic devices, such as field-effect transistors, printed electronics, and

high-resolution display.^[34–36] Up to now, there are a number of methods for microscale patterning of the graphene. Nanoscale-patterned graphene can be directly tailored by focused ion beam without any mask, but it is not an extensive pattern method due to its low processing efficiency for large-area patterns.^[37,38] Graphene based inks for direct inkjet printing of graphene patterns is another option with properties of large-scale fabrication and high resolution. Unfortunately, thin graphene inks films consist of nanoscale to microscale graphene flakes exhibit relatively low conductivity due to its discontinuous large-area framework compared with chemical vapor deposition (CVD) grown graphene.^[39,40] Patterned CVD-grown graphene can be obtained by pre patterning of catalytic metal on insulation substrates, while the patterned catalytic metal suffers from deformation after the high-temperature treatment which influence the profile of the patterned graphene. Besides that, complicated and time consuming transfer processes afterward is needed to transfer the patterned graphene to the desired substrate by using a supporting layer for its further application.^[41,42] Conventional photolithography combined with plasma etching is another method for microscale patterning of the CVD-grown graphene.^[43–46] In this case, the transfer process is needed before the lithography patterning. Poly methyl methacrylate/methacrylic acid (PMMA) is the most commonly used (Supporting Information), but always caused polymer residue.^[47,48] The two separate steps of the patterning and transfer with different materials used

Y. Chen, N. Zhang, Y.-F. Li, Dr. Y.-G. Bi, Y.-Y. Yue, Prof. J. Feng,
Prof. H.-B. Sun
State Key Laboratory of Integrated Optoelectronics College of Electronic
Science and Engineering
Jilin University
2699 Qianjin Street, Changchun 130012, China
E-mail: jingfeng@jlu.edu.cn

Prof. H.-B. Sun
State Key Lab of Precision Measurement Technology and Instruments
Department of Precision Instrument
Tsinghua University
Haidian, Beijing 100084, China

 The ORCID identification number(s) for the author(s) of this article can be found under <https://doi.org/10.1002/adom.201701348>.

DOI: 10.1002/adom.201701348

results in a complicated and unreliable fabrication of the patterned graphene. So far, a simplified fabrication process is still a challenge for the graphene transfer and patterning.

In this work, we demonstrate a simple and reliable transfer-pattern strategy by using a photoresist as both supporting layer for the graphene transfer and photolithographic mask layer for the microscale-patterned graphene electrode. Based on this transfer-pattern strategy, monolayer to tri-layer graphene can be transferred onto desired substrates with ideal microscale patterns. The transfer-patterned monolayer graphene film shows a smooth surface morphology with a surface roughness (Ra) of 0.675 nm due to the effective removal of the residual photoresist. We have fabricated 25 μm line width patterned OLEDs with high precision and uniform lighting areas, which reveals the great potential of the transfer-patterned graphene as electrodes for organic optoelectronic devices, especially for high-resolution flat panel display. Furthermore, transfer-patterned graphene with a scale of ≈ 2 in. demonstrates that this transfer-pattern strategy is suitable for large-scale graphene fabrication, which is important for its practical applications.

2. Results and Discussion

2.1. Transfer and Microscale Pattern of CVD Grown Graphene

Figure 1 shows the schematic illustration of transfer and microscale pattern steps for CVD grown graphene. First, ≈ 1 μm thick of photoresist (S1805G) was spin-coated on a graphene/Cu foil as a supporting layer and Cu foil was subsequently etched in $\text{K}_2\text{S}_2\text{O}_8$, leaving photoresist/graphene

membrane floated over the surface of etchant solution (Figure 1a–c). After that, the photoresist/graphene membrane was subsequently transferred onto desired substrates, such as glass or NOA63/ SiO_2/Si (Figure 1c,d). From here on, two kinds of procedures were applied. As for monolayer graphene electrode, photoresist/graphene directly went into pattern process (Figure 1 d–g). In the case of multilayer graphene electrodes, photoresist was primarily removed in hot acetone leaving graphene on glass substrate (Figure 1d,e), after that, another photoresist/graphene membrane was transferred on it (Figure 1c,e,f). By repeating this transfer process, photoresist of S1805G with specific layers of graphene could stack on glass substrate (Figure 1f). As for graphene pattern, a microscale photomask was used for photoresist/graphene exposure under a stable UV light, the highest resolution of microscale photomasks used is 25 μm (Figure 1d–g/f,g). Then, exposed photoresist was developed in positive photoresist developer to form photoresist microscale pattern which is matched with the corresponding photomask (Figure 1g,h). Ar plasma was used to remove the region of graphene without patterned photoresist protection, and the remaining graphene naturally duplicated the microscale pattern from photoresist. In the last step (Figure 1j,k), patterned photoresist was dissolved in hot acetone, leaving specific layers of microscale-patterned graphene on glass substrate (more specific details of transfer-patterned process are shown in the Experimental Section). Two main components of the photoresist are 2-acetoxy-1-methoxypropane and phenol-formaldehyde resin monomer. Between these two materials, 2-acetoxy-1-methoxypropane acts as the solvent for phenol-formaldehyde resin. As a sort of resin, phenol-formaldehyde resin has a favorable solubility in organic solvent, such

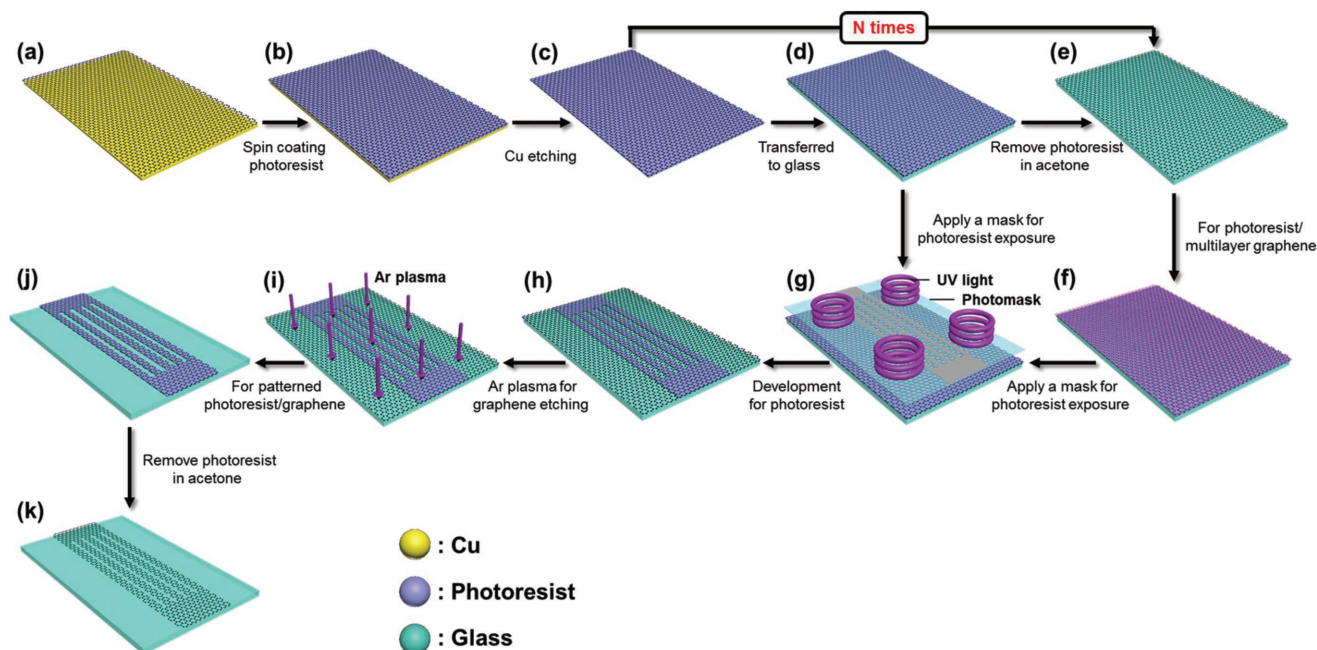


Figure 1. Schematic illustration of patterned graphene fabricated by transfer-pattern strategy. a) Graphene grown on Cu foils, b) photoresist spin coated on graphene/Cu, c) Cu was chemically etched, leaving photoresist/graphene, d) photoresist/graphene was transferred onto glass substrate, e) photoresist was removed in acetone, f) another photoresist/graphene was covered on graphene/glass substrate, g,h) lithographic process for photoresist via a microscale photomask, i,j) plasma etching for microscale-patterned graphene, and k) removing photoresist in acetone.

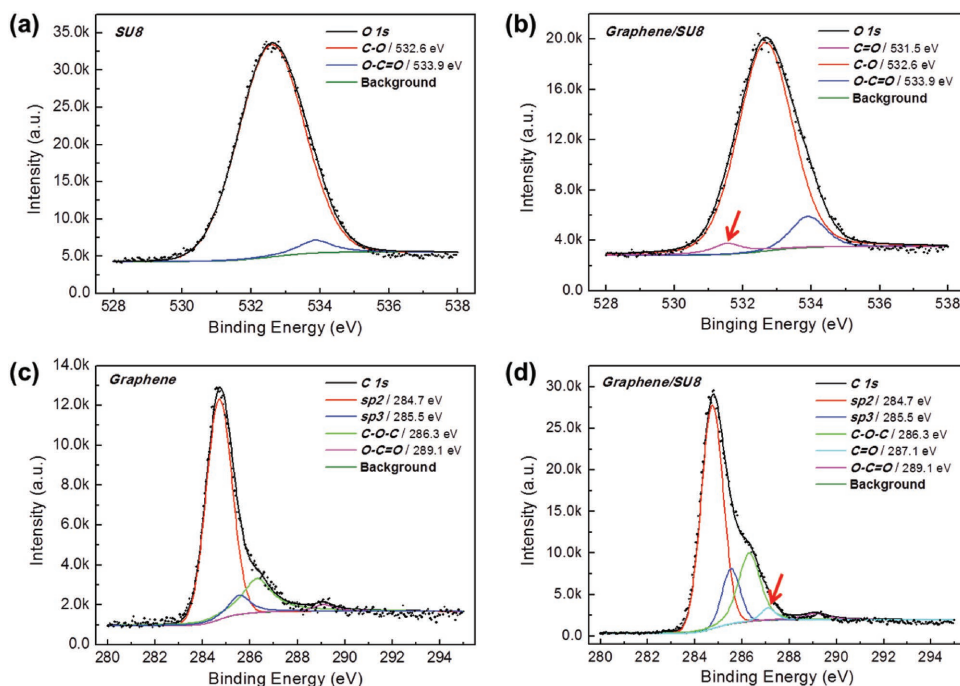


Figure 2. Detailed high-resolution O 1s X-ray photoelectron spectroscopy (XPS) spectra of a) SU-8 and b) graphene/SU-8; C 1s XPS spectra of c) graphene and d) graphene/SU-8. All these samples are prepared on SiO₂/Si substrate.

as acetone and ethanol.^[31] Therefore, effectively removing photoresist in 60 °C acetone only takes less than 10 s, which dramatically shorten the disposed time of polymer supporting layer (Movie S1, Supporting Information).

Graphene has poor attachment with glass or SiO₂/Si substrates during its transfer-patterned process. The surface morphology of the photoresist/graphene directly transferred onto glass surface (Figure S1, Supporting Information) is obviously inhomogeneous, and photoresist/graphene film partly peels off from glass substrate under air flow. Even worse, graphene on glass substrate peels off in a large area during the graphene pattern process, especially for the development process of photoresist. The poor attachment between graphene and glass causes serious damage for micropatterned graphene. It is known that organic polymers possess a great deal of oxygen functional groups which has strong interaction with carbon materials.^[49,50] Misikin et al. recently proved that pyrenes can be designed as binding groups to adjust the work of separation between graphene and substrate.^[51] Here, we apply ≈140 nm thick of SU-8 polymer spin-coated onto glass as a modification layer (Figure S2, Supporting Information). The photoresist/graphene on SU-8/glass exhibits a homogeneous surface feature, and photoresist/graphene structure maintains integrated under the same air flow (Figure S1, Supporting Information). The chemical composition between graphene and SU-8 was analyzed by high-resolution X-ray photoelectron spectroscopy (XPS) to investigate the chemical bonding related to O 1s and C 1s (Figure 2). The O 1s spectra of SU-8 and graphene/SU-8 (Figure 2a,b) can be de-convoluted into different functional groups of C–O (532.6 eV), O–C=O (533.9 eV), and C=O (531.5 eV),^[52] while the unique C=O bonds just appears in graphene/SU-8 system. To further confirm that

C=O bonds derive from the bonding between graphene and SU-8 rather than graphene itself, the C1s XPS spectra of graphene and graphene/SU-8 were investigated (Figure 2c,d). The high-resolution C 1s spectra of graphene can be de-convoluted into sp² (284.7 eV), sp³ (285.5 eV), C–O–C (286.3 eV), and O–C=O (289.1 eV).^[53] Noticeably, C 1s peak decomposition of graphene/SU-8 system also shows an additional C=O (287.1 eV) bonds well matched with the O 1s analysis result, attesting to the fact that C=O bonds have formed at the interface of graphene and SU-8. Graphene on SU-8 shows strong interaction which insures microscale-patterned graphene being smooth and integrated. Corresponding real object schematic of the transfer-patterned process based on SU-8/glass substrate is shown in Figure S3 (Supporting Information).

2.2. Characteristics of the Transfer-Patterned Graphene Electrodes

The edges of patterned graphene from monolayer to tri-layer were characterized by optical microscopy, as shown in Figure 3a–c, respectively. The brighter areas in the vision field are graphene electrodes while the dark areas correspond to the bare glass where graphene is etched away by Ar plasma. The sharp and straight boundaries between these two areas demonstrate the high quality of the patterned graphene by the transfer-patterned process. The monolayer graphene electrode shows a clean and smooth surface morphology with negligible polymer residues. The white spots are regard as graphene nucleation points, and the grain size is around 5 μm. Atomic force microscopy (AFM) images of the monolayer, bilayer, and tri-layer graphene are shown in Figure 3d–f, respectively. The selected large area of each sample is 40 × 40 μm², and the corresponding surface

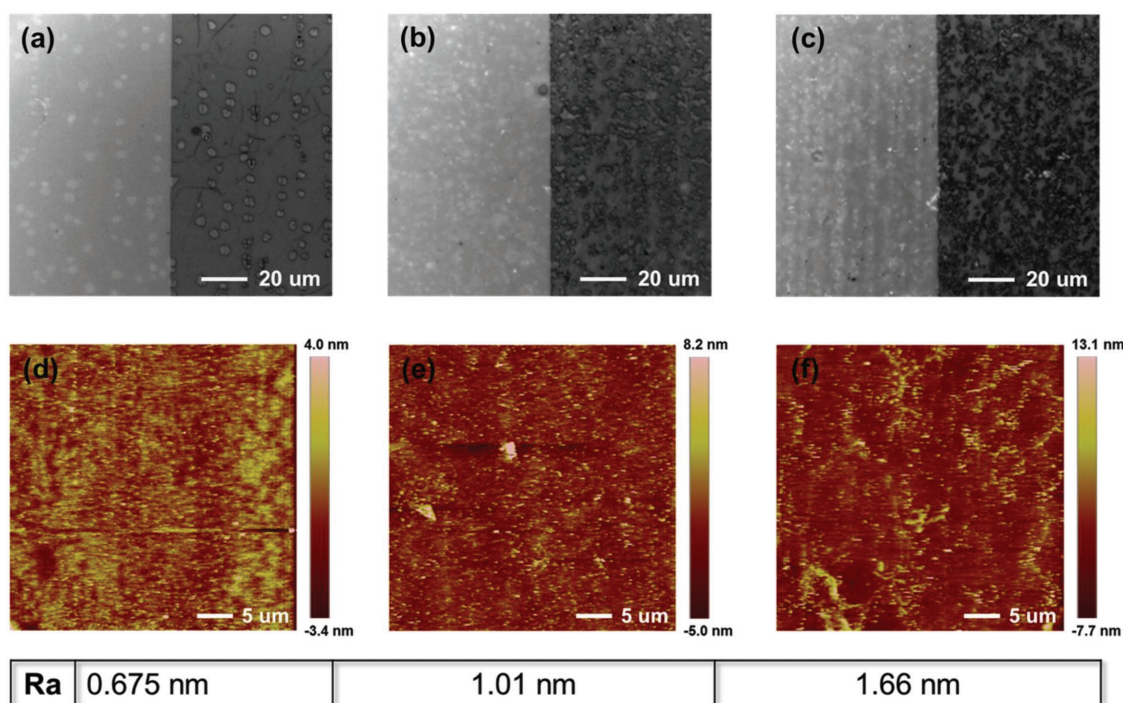


Figure 3. Optical microscopy images of the edges of patterned a) monolayer, b) bilayer, and c) tri-layer graphene. AFM topographic images of d) monolayer, e) bilayer, and f) tri-layer graphene, respectively. Corresponding surface roughness (R_a) is given in the bottom table.

roughness (R_a) is shown in the bottom table of Figure 3. The photoresist transfer-patterned monolayer graphene film shows an extremely low R_a of 0.675 nm, which is five times lower than that of the PMMA-transferred monolayer graphene (Figure S4, Supporting Information). As for bilayer and tri-layer graphene, R_a slightly rises to 1.01 and 1.66 nm. The increased R_a might be caused by the interlayer contamination from $K_2S_2O_8$ etchant during the repeated transfer process, which is still much lower than PMMA-transferred monolayer graphene (3.42 nm).

Raman spectroscopy was used to characterize the atomic structure and electronic properties of various layers of patterned graphene electrodes (Figure 4a). The peak position of G and 2D bands are located at 1589 and 2682 cm^{-1} , and the intensity ratio of $I_{2D}/I_G \approx 2$ indicating that as-grown graphene is single layer.^[31,33] As for bilayer and tri-layer graphene, the intensities of G and 2D peaks both increase with the number of layers, and the values of I_{2D}/I_G maintain around 2 which is different from the ABA-stacked bilayer and tri-layer graphene.^[54,55] Considering that the bilayer and tri-layer graphene in this work are stacked by monolayer graphene through the photoresist transfer-patterned process, adjacent layers of graphene likely exist a random twist angle. Previous researches have reported that Raman spectra of stacked graphene show a rich variation in the peak intensities and shapes. In the high-angle arrangement ($>13^\circ$), Raman spectra of bilayer graphene display closed to those of monolayer graphene.^[56,57] Negligible intensity of D band (1347 cm^{-1} for tri-layer graphene) has demonstrated that photoresist has been effectively removed and no obvious damage was generated during the transfer-patterned process. Raman characterizations of graphene quality is consistent with the XPS data of graphene C 1s analysis result

(Figure 2c), C sp^2 and sp^3 compositions are 71.1% and 7.4%, respectively. The interference signal peaks in Raman spectra around 1458 and 1523 cm^{-1} belong to SU-8/glass substrate.

Figure 4b shows the transmittance spectra of monolayer, bilayer, and tri-layer graphene, and the inset is the photograph of actual samples on SU-8/glass substrates. The transmittance of the monolayer graphene electrode at $\lambda = 550$ nm is about 97.4%, which is comparable with ideal monolayer graphene (97.7%), indicating that photoresist is nearly fully removed from the surface of graphene.^[58] Transmittance for bilayer and tri-layer graphene electrodes decrease about $\approx 3\%$ for each layer, and the value of tri-layer graphene is still higher than 91%.^[59] Compared with ITO electrode, monolayer to tri-layer graphene exhibit higher transmittance at wavelength range of 400–500 nm.^[32,60] Sheet resistance variety of various layers of patterned graphene is shown in Figure 4c, and 10 randomly selected points of each sample were measured for acquiring a universal result. The mean sheet resistances for monolayer to tri-layer graphene are 444, 215, and 168 $\Omega \square^{-1}$, respectively. The value of monolayer graphene transfer-patterned by photoresist is much lower than PMMA-transferred monolayer graphene reported in previous literature (≈ 0.8 –1 $K\Omega \square^{-1}$),^[60] which similarly confirms that photoresist used in this work is an efficient mediator for graphene transfer and pattern. In order to further reduce the sheet resistance, 5 nm MoO_3 layer as p-type dopant was thermally evaporated onto graphene surface in high vacuum, and the corresponding sheet resistances are reduced to 351, 190, and 145 $\Omega \square^{-1}$, respectively. In addition, the sheet resistance for the graphene electrodes doped by MoO_3 layer show a smaller standard deviation of 3.6–7.5 $\Omega \square^{-1}$ compared with pristine graphene (7.3–57.6 $\Omega \square^{-1}$), proving that MoO_3 doped graphene has a more uniform electrical property.

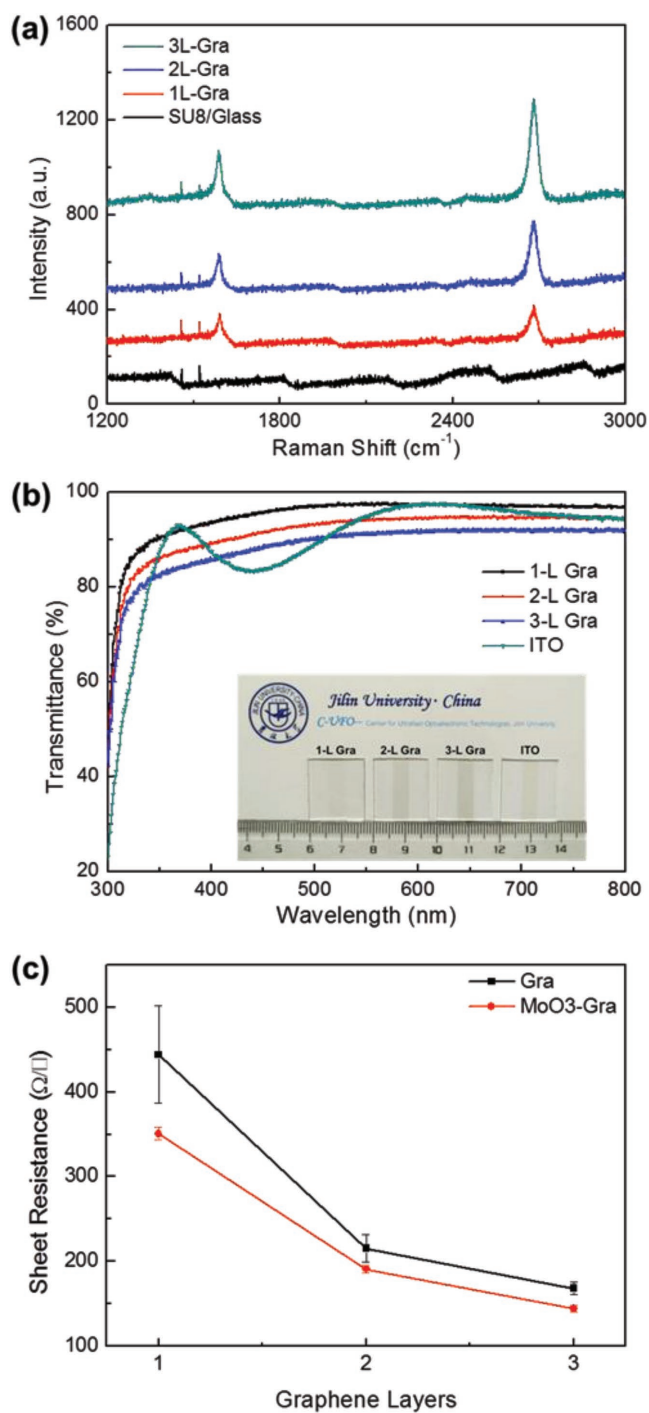


Figure 4. a) Raman spectra of monolayer, bilayer, and tri-layer graphene and the SU-8/glass substrate. b) Transmittance spectra of patterned monolayer, bilayer, and tri-layer graphene and ITO electrode. c) Sheet resistance of pristine graphene and MoO₃ doped graphene with different numbers of graphene layers. Inset of (b) is a photograph of corresponding test samples.

2.3. Characteristics of the OLEDs Based on Transfer-Patterned Graphene Electrodes

At first, we fabricated a lighting area of $0.2 \times 0.2 \text{ cm}^2$ phosphorescent green OLEDs using photoresist transfer-patterned

full graphene as the anodes on glass substrate. The Fermi level of MoO₃ doped monolayer graphene down-shifts 0.23 eV compared to pristine graphene, inducing a nearly perfect energy alignment for the hole injection and transporting (Figure S6, Supporting Information). Furthermore, poly(3,4-ethylenedioxythiophene) : poly(styrenesulfonate) (PEDOT:PSS) spin-coated on MoO₃/graphene exhibits better wetting property and more uniform surface morphology (Figure S7, Supporting Information). After 5 nm MoO₃ was thermal evaporated onto graphene anode, PEDOT:PSS was spin-coated on MoO₃/graphene or ITO anodes as a smooth and hole transport layer, another 10 nm MoO₃ layer is used to further enhance the hole transport to N,N'-bis(naphthalen-1-yl)-N,N'-bis(phenyl)benzidine (NPB). The emissive layer of the green OLEDs is methyl cyclopentenolone (Mcp) doped with tris[2-phenylpyridinato-C²,N] iridium(III) (Ir(ppy)₃). 1,3,5-tri(1-phenyl-1H-benzo[d]imidazol-2-yl)phenyl (TPBi) is used as electron transport layer and Ca/Ag as composite cathode. Figure 5a shows the structure schematic diagram of green OLEDs based on patterned graphene anode.

The performances of the OLEDs with patterned monolayer, bilayer, and tri-layer graphene, and the ITO anode on glass substrate are summarized in Figure 5b–d. It is obvious that current density is significantly increased for the OLEDs with increasing layers of graphene from monolayer to tri-layer graphene devices because of the improved conductivity (Figure 5b). The sheet resistance of ITO is only $\approx 15 \Omega \square^{-1}$, and the corresponding device shows the highest current density. The sheet resistance of doped bilayer graphene is $\approx 190 \Omega \square^{-1}$, which is an order of magnitude higher than ITO. Corresponding current density of the OLEDs based on the bilayer graphene is clearly lower than that of the ITO-based devices. A more effective doping method should be explored to further lower the sheet resistance to maintain the large-area emission uniformity of the graphene-based OLEDs.

The maximum luminance for monolayer, bilayer, and tri-layer graphene devices are 17 050, 63 700, and 75 370 cd m^{-2} , respectively (Figure 5c). The highest luminance of tri-layer graphene device is comparable with that of ITO anode. The maximum current efficiency is achieved for OLEDs with bilayer graphene anode, which is 33 cd A^{-1} at 6 V and comparable to the ITO-based OLEDs (34.6 cd A^{-1}) (Figure 5c). The power efficiency and external quantum efficiency (EQE) values of monolayer to tri-layer graphene based OLEDs are shown in Figure S8 (Supporting Information). The corresponding highest values are 12, 17.59, and 14.72 lm W^{-1} for power efficiency, and 7.57%, 9.39%, and 8.25% for EQE, respectively. Among these devices, bilayer graphene shows the best performance. Highest sheet resistance of the monolayer graphene results in its lowest efficiency. The lower efficiency of the tri-layer graphene based OLEDs can be attributed to its relatively high roughness and low transmittance. Graphene-based OLEDs show the boarder emission peaks compared to that of ITO-based OLEDs, as can be seen from the EL spectra in Figure 5d. Inset of Figure 5d shows polar plots of the emission intensity for the OLEDs based on the bilayer graphene and ITO. The bilayer graphene-based OLEDs exhibit a slower decreased of the emission intensity compared to the ITO-based OLEDs with the increased viewing angles.

Flexible OLEDs based on the bilayer graphene anode was fabricated on NOA63 polymer film. The functional layers deposited on bilayer graphene anode/NOA63/SiO₂/Si substrate

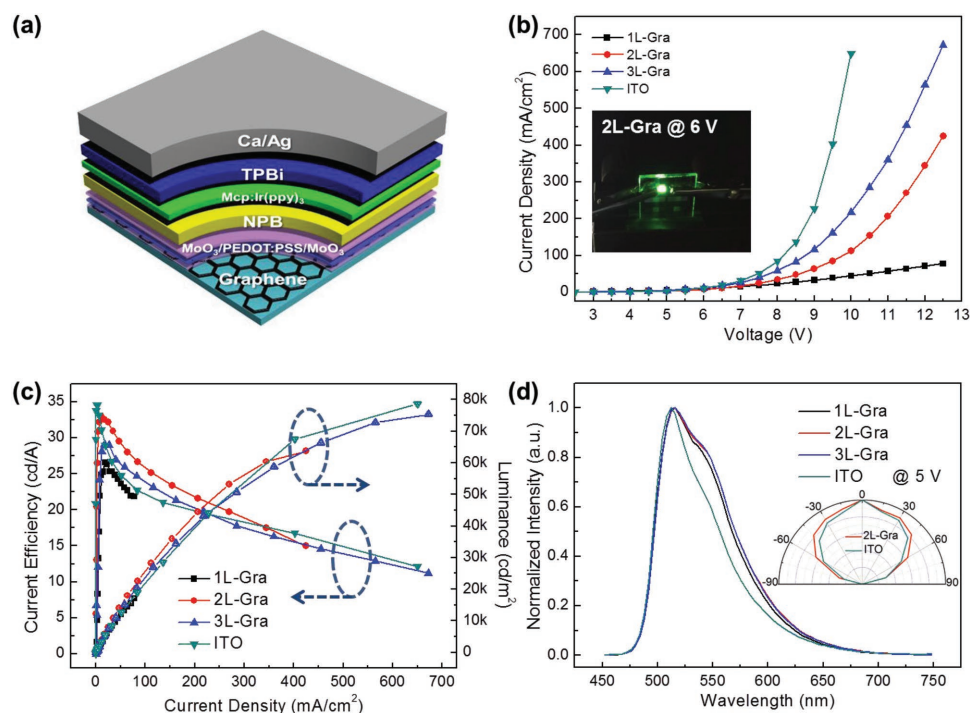


Figure 5. a) Structure schematic diagram of green OLEDs with monolayer graphene anode. b) Current–voltage, c) luminance and current efficiency–current density, and d) EL spectra of rigid OLEDs based on monolayer to tri-layer graphene and ITO anodes. Inset of (b) shows photograph of bilayer graphene based OLEDs driven at the voltage of 6 V. Inset of (d) is EL intensity of OLEDs based on bilayer graphene and ITO anodes as a function of emission angle.

are same as the rigid OLEDs. After that, the entire OLEDs on NOA63 films were peeled off from the SiO₂/Si substrate. **Figure 6a** is the photograph of flexible OLEDs fabricated on bilayer graphene anode at driven voltage of 8 V. The device was attached to a cartridge with radius of 2 mm, and bright green light emission from its surface can be observed. The luminance–voltage and current efficiency–current density characteristics of the flexible device are shown in **Figure 6b**. The best flexible OLEDs based on bilayer graphene anode exhibit a high current efficiency of 31.4 cd A⁻¹, which is comparable to the rigid devices. The stable and bright lighting area at different bending radius further demonstrates the excellent mechanical flexibility of flexible OLEDs based on the graphene anode (**Figure S9**, Supporting Information). These results have further

proved that the transfer-patterned graphene is applicable to the efficient flexible OLEDs.

The patterned OLEDs with high resolution have been realized by using the transfer-patterned graphene anode. **Figure 7a–c** show the optical images of microscale-patterned photomasks with line wide of 100, 50, and 25 μm, respectively. The corresponding scanning electron microscope (SEM) images of microscale-patterned graphene electrodes are shown in **Figure 7d–f**. Transmittance of patterned monolayer graphene strips with different line width is shown in **Figure S10** (Supporting Information). The patterned OLEDs based on the microscale-patterned graphene anodes with line width of 100, 50, and 25 μm, respectively are shown in **Figure 7g–i**. All these devices show bright and uniform lighting areas, as well as the feature of high contrast. This OLEDs array

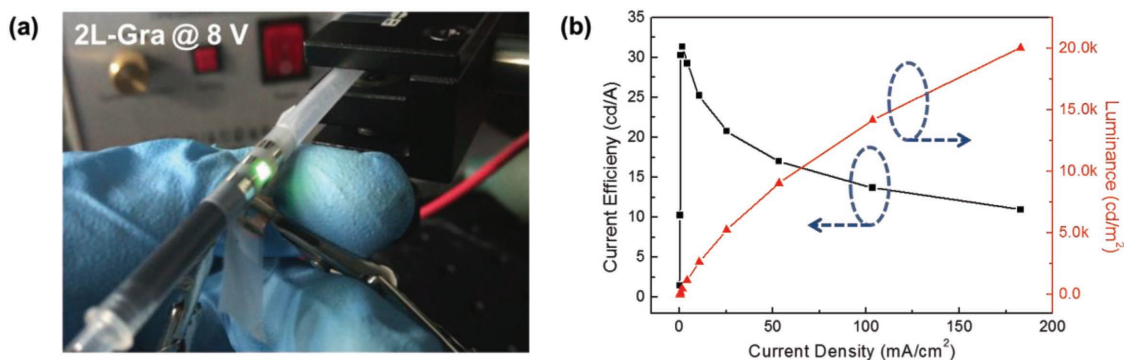


Figure 6. a) Photograph of flexible OLEDs with bilayer graphene on thick NOA63 film at driven voltage of 8 V; the bending radius is 2 mm. b) Luminance and current efficiency as a function of current density for flexible OLEDs based on bilayer graphene anode.

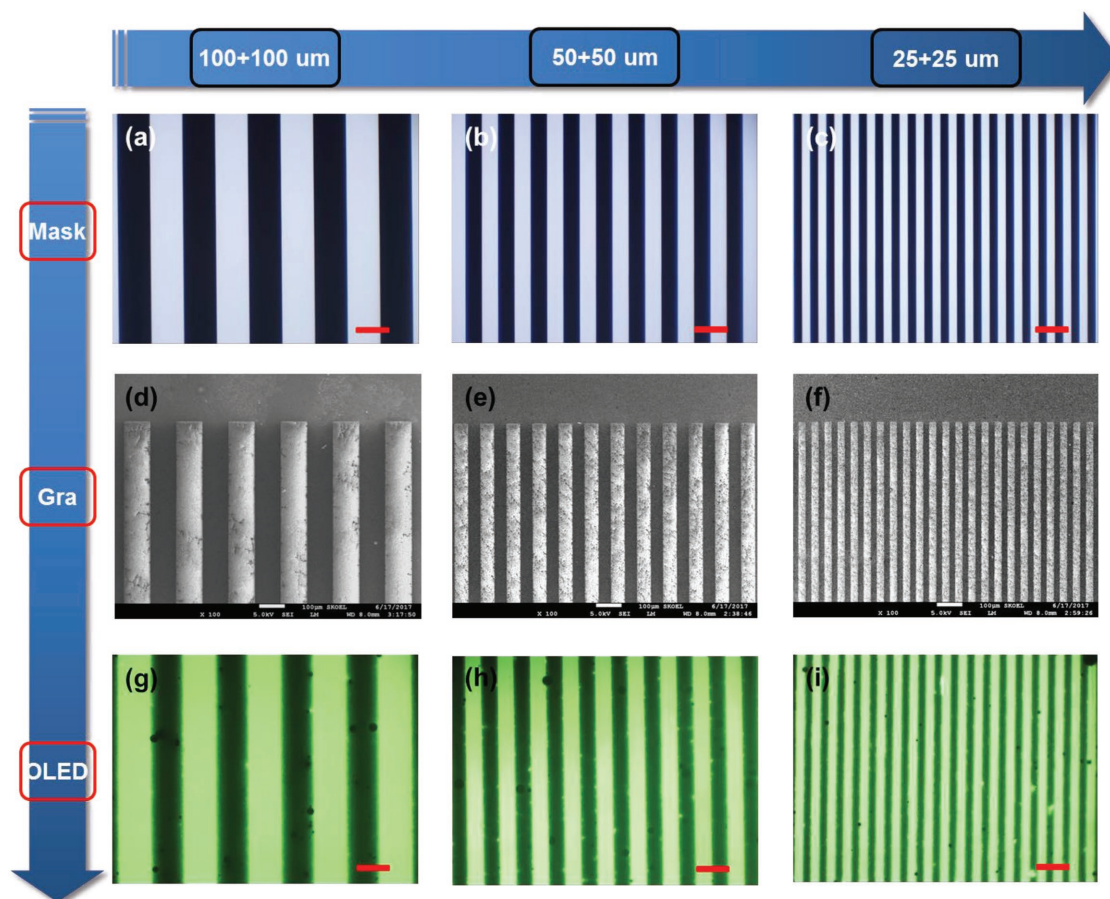


Figure 7. a–c) OM images of photomask with a) 100 μm , b) 50 μm , and c) 25 μm line width, respectively. d–f) SEM images of microscale-patterned monolayer graphene anodes. OM images of OLEDs based on microscale-patterned monolayer graphene anodes with g) 100 μm , h) 50 μm , and i) 25 μm lighting line width. Scale bar is 100 μm .

has demonstrated the great potential of graphene used as microscale electrodes for organic optoelectronic devices, especially for high-resolution flat panel display. Moreover, the transfer-pattern process is applicable to large-area graphene transfer and pattern. Figure S11 (Supporting Information) shows the photographs of ≈ 2 in. photomask and corresponding bilayer graphene pattern. Large-area graphene pattern with high integrity and fidelity can be observed. Furthermore, the OLED with emitting area reaches to 1 cm^2 based on hexagonal patterned bilayer graphene anode is fabricated, and corresponding photograph is shown in Figure S12 (Supporting Information). Therefore, the transfer-pattern strategy reported here has great potential for large-area application of graphene-based electronic and optoelectronic devices.

3. Conclusion

In summary, we have demonstrated a transfer-pattern strategy for clean transfer and microscale patterning of graphene by using a photoresist as both supporting layer for the graphene transfer and photolithographic mask layer for the microscale-patterned graphene electrode. The transfer-patterned graphene exhibits excellent properties of smooth surface morphology, low sheet resistance, and high optical transmittance. Both

rigid and flexible OLEDs with the transfer-patterned graphene anode exhibit comparable efficiency to the OLEDs based on ITO anode. OLEDs array with 25 μm line width has been realized, which demonstrates the great potential of graphene as microscale electrodes for the flat panel display. Moreover, a scale of ≈ 2 in. patterned graphene well demonstrates the large-area application of the transfer-patterned graphene. The clean transfer and high-quality microscale pattern of the graphene based on the transfer-pattern strategy simplifies the fabrication procedures of the patterned graphene electrode and promotes its applications in electronic and optoelectronic devices.

4. Experimental Section

CVD Growth and Transfer-Patterning of the Graphene: Copper foils (25 μm , Alfa Aesar) were disposed in 5% vol HCl for 5 min to remove the copper oxides coverage before they were inserted into a quartz tube of a CVD system. Then, the copper foils were heated to 1000 $^\circ\text{C}$ in 10 sccm H_2 and 100 sccm Ar forming gas for 40 min to enlarge the grain size of copper. After that, 1 sccm CH_4 was introduced for 10 min to form graphene nucleation site, followed 3 sccm CH_4 was injected to grow full graphene film within 40 min. Finally, copper films were rapidly cooled to room temperature. As for graphene transfer and microscale pattern, ≈ 1 μm thick S1805G positive photoresist (Dow Chemical, 10407990) was spin-coated on copper foils as the transfer-patterned

mediator. Graphene grown on the other side of copper was destroyed by Ar plasma for 20 min, and then copper foil was chemically dissolved in $K_2S_2O_8$ saturated solution for about 2 h, leaving S1805G/graphene membrane floated over the surface of etchant solution. The S1805G/graphene membrane was washed with deionized water for three times, followed by transfer onto a glass substrate spin-coated with ≈ 140 nm SU-8 (2025, MicroChem Corp.) polymer (the substrate is NOA63/SiO₂/Si for flexible device). In order to obtain multilayer graphene, photoresist was first removed in 60 °C acetone for only few seconds (60 °C alcohol was also used to remove acetone, followed by deionized water wash), another photoresist/graphene membrane was then transferred onto the prior graphene film. By cycling this section, photoresist with specific layers of graphene stacks on desired substrates can be achieved. The photomask was tightly covered onto the surface of photoresist under a stable UV-light lamp (250 mW) with exposure time of 15 s (the vertical distance between photomask and UV light is around 20 cm), the wavelength of used UV light is 254 nm, purchased from Philips Lighting. As for the microscale-patterned photomask with strips, it is chrome-plated and custom-made from Micro-Nano Commercial and Trading Co., Ltd., Shenzhen, China. Subsequently, exposed photoresist was developed in positive photoresist developer (ZX-238) for a few seconds to form patterned photoresist. Ar plasma was used to destroy graphene without the protection of patterned photoresist; 8 min is a proper processing time for patterns of bilayer graphene. At last, patterned photoresist was similarly removed in hot acetone, leaving patterned graphene with specific layers on desired substrates. As for contrast PMMA transferred monolayer, ≈ 300 nm PMMA supporting layer was immersed in 60 °C acetone for 30 min.

Fabrication of Rigid and Flexible OLEDs: First, p-type doping of transfer-patterned graphene electrode was performed by thermally evaporating 5 nm MoO₃ layer on its surface in a high vacuum chamber with base pressure lower than 5×10^{-4} Pa. About 40 μ m thick filtrated PEDOT:PSS (Xi'an p-OLED, China) stock solution was spin-coated on doped graphene and ITO film at 3000 r.p.m. for 30 s; PEDOT:PSS was then annealed on a hot plate at 100 °C for 30 min. After that, both graphene/MoO₃ and ITO anodes with PEDOT:PSS layer were loaded into a high vacuum chamber for the deposition of subsequent function layers, including a 10 nm MoO₃ hole injection layer, a 40 nm NPB hole transportation layer, a 20 nm Mcp:Ir(ppy)₃ (10% wt) light emission layer, a 40 nm TPBi electron transportation layer, and a 2 nm Ca/80 nm Ag cathode. The light area of as-fabricated OLEDs is 2×2 mm² which is defined by the size of cathode. The functional organic and cathode layers were sequentially deposited on the whole 2×2 mm² device area without the shadow mask. As for flexible OLEDs, the substrate of NOA63 (Norland Products, Inc.) film was spin-coated on the octylsilane (OTS) modified SiO₂/Si at 6000 r.p.m. for 30 s, subsequently exposed under a stable UV-light lamp (250 mW) for 2 min. After the whole OLEDs structure was deposited, NOA63 film with entire device was peeled from SiO₂/Si.

Characterizations of the Graphene and OLEDs: Optical microscope (OM) ($\times 50$ telephoto lens), AFM (Dimension Icon, Bruker Corporation), and SEM (JSM-7500F, JEOL) were used to characterize the surface of transfer-patterned graphene electrodes with different numbers of layers on SU-8/glass substrate. UV-vis spectrophotometer (UV-2550, SHIMADZU) and Raman spectrophotometer (LabRAM HR Evolution, HORIBA, with 532 nm laser) were used to measure the absorption spectra and Raman spectra, respectively. Corresponding sheet resistance was measured by a 4-probe resistivity measurement system (RTS-5 Type, China). XPS was used to analyze the surface chemical composition of SU-8, graphene, and graphene/SU-8, while UPS was used to characterize the interface energetics of graphene, MoO₃-graphene, and PEDOT:PSS (PREVAC XPS/ultraviolet photoelectron spectroscopy (UPS) System). The current density and luminance characteristics of the rigid and flexible OLEDs were measured by using a Keithley 2400 programmable voltage-current source and Photo Research PR-655 spectrophotometer. The photographs of microscale-patterned photomask and OLEDs were taken by OM with $\times 10$ objective lens.

Supporting Information

Supporting Information is available from the Wiley Online Library or from the author.

Acknowledgements

This work was supported by the National Key Research and Development Program of China and National Natural Science Foundation of China (NSFC) under Grants #2017YFB0404501, #61675085, #61505065, #61605056 and #61705075.

Conflict of Interest

The authors declare no conflict of interest.

Keywords

microscale-patterned graphene, organic light-emitting devices, patterning strategy

Received: December 12, 2017

Revised: February 27, 2018

Published online:

- [1] H. H. Chou, C. H. Cheng, *Adv. Mater.* **2010**, *22*, 2468.
- [2] H. Wang, L. S. Xie, Q. Peng, L. Q. Meng, Y. Wang, Y. P. Yi, P. F. Wang, *Adv. Mater.* **2014**, *26*, 5198.
- [3] B. Q. Liu, L. Wang, D. Y. Gao, J. H. Zou, H. L. Ning, J. B. Peng, Y. Cao, *Light: Sci. Appl.* **2016**, *5*, e16137.
- [4] E. Ahmed, T. Earmme, S. A. Jenekhe, *Adv. Funct. Mater.* **2011**, *21*, 3889.
- [5] S. Reineke, F. Lindner, G. Schwartz, N. Seidler, K. Walzer, B. Lüssem, K. Leo, *Nature* **2009**, *459*, 234.
- [6] Y. H. Chen, D. G. Ma, H. D. Sun, J. S. Chen, Q. X. Guo, Q. Wang, Y. B. Zhao, *Light: Sci. Appl.* **2016**, *5*, e16042.
- [7] Q. S. Zhang, B. Li, S. P. Huang, H. Nomura, H. Tanaka, C. Adachi, *Nat. Photonics* **2014**, *8*, 326.
- [8] H. J. Bolink, E. Coronado, D. Repetto, M. Sessolo, E. M. Barea, J. Bisquert, G. Garcia-Belmonte, J. Prochazka, L. Kavan, *Adv. Funct. Mater.* **2008**, *18*, 145.
- [9] D. D. Zhang, L. Duan, Y. G. Zhang, M. H. Cai, D. Q. Zhang, Y. Qiu, *Light: Sci. Appl.* **2015**, *4*, e232.
- [10] H. Uoyama, K. Goushi, K. Shizu, H. Nomura, C. Adachi, *Nature* **2012**, *492*, 234.
- [11] D. Yin, J. Feng, R. Ma, Y. F. Liu, Y. L. Zhang, X. L. Zhang, Y. G. Bi, Q. D. Chen, H. B. Sun, *Nat. Commun.* **2016**, *7*, 11573.
- [12] S. D. Yambem, A. Haldar, K. S. Liao, E. P. Dillon, A. R. Barron, S. A. Curran, *Sol. Energy Mater. Sol. Cells* **2011**, *95*, 2424.
- [13] Y. B. Bi, J. Feng, J. H. Ji, Y. Chen, Y. S. Liu, Y. F. Li, Y. F. Liu, X. L. Zhang, H. B. Sun, *Nanoscale* **2016**, *8*, 10010.
- [14] J. Lee, P. Lee, H. Lee, D. Lee, S. S. Lee, S. H. Ko, *Nanoscale* **2012**, *4*, 6408.
- [15] M. G. Kang, T. Xu, H. J. Park, X. G. Luo, L. J. Guo, *Adv. Mater.* **2010**, *22*, 4378.
- [16] Y. Kim, T. I. Ryu, K. H. Ok, M. G. Kwak, S. Park, N. G. Park, C. J. Han, B. S. Kim, M. J. Ko, H. J. Son, J. W. Kim, *Adv. Funct. Mater.* **2015**, *25*, 4580.
- [17] D. Alemu, H. Y. Wei, K. C. Hod, C. W. Chu, *Energy Environ. Sci.* **2012**, *5*, 9662.

- [18] S. I. Na, S. S. Kim, J. Jo, D. Y. Kim, *Adv. Mater.* **2008**, *20*, 4061.
- [19] K. Fehse, K. Walzer, K. Leo, W. Lövenich, A. Elschner, *Adv. Mater.* **2007**, *19*, 441.
- [20] D. H. Zhang, K. Ryu, X. L. Liu, E. Polikarpov, J. Ly, M. E. Tompson, C. W. Zhou, *Nano Lett.* **2006**, *6*, 1880.
- [21] C. H. Wang, C. Y. Li, L. Ting, X. L. Xu, C. F. Wang, *Microchim. Acta* **2006**, *152*, 233.
- [22] R. R. W. Simendinger, C. D. H. Shimoda, L. Fleming, B. Stoner, O. Zhou, *Appl. Phys. Lett.* **2000**, *76*, 1668.
- [23] Y. S. Ly, K. S. Kim, H. T. Kim, S. Y. Jung, M. S. Lee, *J. Appl. Electrochem.* **2005**, *35*, 567.
- [24] J. T. Lim, H. Lee, H. Cho, B. H. Kwon, N. S. Cho, B. K. Lee, J. Park, J. Kim, J. H. Han, J. H. Yang, B. G. Yu, C. S. Hwang, S. C. Lim, J. I. Lee, *Sci. Rep.* **2015**, *5*, 17748.
- [25] J. B. Wu, M. Agrawal, H. A. Becerril, Z. N. Bao, Z. F. Liu, Y. S. Chen, P. Peumans, *ACS Nano* **2010**, *4*, 43.
- [26] H. Meng, J. X. Luo, W. Wang, Z. J. Shi, Q. L. Niu, L. Dai, G. G. Qin, *Adv. Funct. Mater.* **2013**, *23*, 3324.
- [27] J. H. Kim, J. Seo, D. G. Kwon, J. A. Hong, J. Hwang, H. K. Choi, J. Moon, J. I. Lee, D. Y. Jung, S. Y. Choi, Y. Park, *Carbon* **2014**, *79*, 623.
- [28] T. H. Han, Y. Lee, M. R. Choi, S. H. Woo, S. H. Bae, B. H. Hong, J. H. Ahn, T. W. Lee, *Nat. Photonics* **2012**, *6*, 105.
- [29] J. Lee, T. H. Han, M. H. Park, D. Y. Jung, J. Seo, H. K. Seo, H. Cho, E. Kim, J. Chung, S. Y. Choi, T. S. Kim, T. W. Lee, S. Yoo, *Nat. Commun.* **2016**, *7*, 11791.
- [30] X. Y. Zhang, S. H. Sun, X. J. Sun, Y. R. Zhao, L. Chen, Y. Yang, W. Lü, D. B. Li, *Light: Sci. Appl.* **2016**, *5*, e16130.
- [31] Z. K. Zhang, J. H. Du, D. D. Zhang, H. D. Sun, L. C. Yin, L. P. Ma, J. S. Chen, D. G. Ma, H. M. Cheng, W. C. Ren, *Nat. Commun.* **2017**, *8*, 14560.
- [32] W. H. Wang, R. X. Du, X. T. Guo, J. Jiang, W. W. Zhao, Z. H. Ni, X. R. Wang, Y. M. You, Z. H. Ni, *Light: Sci. Appl.* **2017**, *6*, e17113.
- [33] N. Li, S. Oida, G. S. Tulevski, S. J. Han, J. B. Hannon, D. K. Sadana, T. C. Chen, *Nat. Commun.* **2013**, *4*, 2294.
- [34] G. Jo, M. Choe, C. Y. Cho, J. H. Kim, W. Park, S. Lee, W. K. Hong, T. W. Kim, S. J. Park, B. H. Hong, Y. H. Kahng, T. Lee, *Nanotechnology* **2010**, *21*, 175201.
- [35] W. Liu, B. L. Jackson, J. Zhu, C. Q. Miao, C. H. Chung, Y. J. Park, K. Sun, J. Woo, Y. H. Xie, *ACS Nano* **2010**, *4*, 3927.
- [36] J. W. Shin, J. H. Han, H. Cho, J. Moon, B. H. Kwon, S. Cho, T. Yoon, T. S. Kim, M. Suemitsu, J. I. Lee, N. S. Cho, *2D Mater.* **2018**, *5*, 014003.
- [37] D. C. Bell, M. C. Lemme, L. A. Stern, J. R. Williams, C. M. Marcus, *Nanotechnology* **2009**, *20*, 455301.
- [38] J. Kotakoski, C. Brand, Y. Lilach, O. Cheshnovsky, C. Mangler, M. Arndt, J. C. Meyer, *Nano Lett.* **2015**, *15*, 5944.
- [39] L. Huang, Y. Huang, J. J. Liang, X. J. Wan, Y. S. Chen, *Nano Res.* **2011**, *4*, 675.
- [40] E. B. Secor, P. L. Prabhumirashi, K. Puntambekar, M. L. Geier, M. C. Hersam, *J. Phys. Chem. Lett.* **2013**, *4*, 1347.
- [41] Y. H. Lee, J. H. Lee, *Appl. Phys. Lett.* **2009**, *95*, 143102.
- [42] Q. Q. Zhuo, Q. Wang, Y. P. Zhang, D. Zhang, Q. L. Li, C. H. Gao, Y. Q. Sun, L. Ding, Q. J. Sun, S. D. Wang, J. Zhong, X. H. Sun, S. T. Lee, *ACS Nano* **2015**, *9*, 594.
- [43] M. K. Choi, I. Park, D. C. Kim, E. Joh, O. K. Park, J. Kim, M. Kim, C. Choi, J. Yang, K. W. Cho, J. H. Hwang, J. M. Nam, T. Hyeon, J. H. Kim, D. H. Kim, *Adv. Funct. Mater.* **2015**, *25*, 7109.
- [44] W. J. Hyun, E. B. Secor, M. C. Hersam, C. D. Frisbie, L. F. Francis, *Adv. Mater.* **2015**, *27*, 109.
- [45] L. H. Liu, G. Zorn, D. G. Castner, R. Solanki, M. M. Lerner, M. D. Yan, *J. Mater. Chem.* **2010**, *20*, 5041.
- [46] P. Ahlberg, M. Hinnemo, M. Song, X. Gao, J. Olsson, S. L. Zhang, Z. B. Zhang, *Appl. Phys. Lett.* **2015**, *107*, 203104.
- [47] Y. C. Lin, C. C. Lu, C. H. Yeh, C. Jin, K. Suenaga, P. W. Chiu, *Nano Lett.* **2012**, *12*, 414.
- [48] K. J. Lee, K. Ihm, Y. Kumar, J. Baik, M. Yang, H. J. Shin, T. H. Kang, S. Chung, B. H. Hong, *Nanoscale* **2014**, *6*, 1474.
- [49] J. W. Suk, W. H. Lee, J. Lee, H. Chou, R. D. Piner, Y. F. Hao, D. Akinwande, R. S. Ruoff, *Nano Lett.* **2013**, *13*, 1452.
- [50] A. Pirkle, J. Chan, A. Venugopal, D. Hinojos, C. W. Magnuson, S. M. Donnell, L. Colombo, E. M. Vogel, R. S. Ruoff, R. M. Wallace, *Appl. Phys. Lett.* **2011**, *99*, 122108.
- [51] M. Z. Miskin, C. Sun, I. Cohen, W. R. Dichtel, P. L. McEuen, *Nano Lett.* **2018**, *18*, 449.
- [52] M. A. Beluomini, J. L. da Silva, G. C. Sedenho, N. R. Stradiotto, *Talanta* **2017**, *165*, 231.
- [53] M. C. Hsiao, S. H. Liao, M. Y. Yen, C. C. Teng, S. H. Lee, N. W. Pu, C. A. Wang, Y. Sung, M. D. Ger, C. C. M. Ma, M. H. Hsiao, *J. Mater. Chem.* **2010**, *20*, 8496.
- [54] A. C. Ferrari, J. C. Meyer, V. Scardaci, C. Casiraghi, M. Lazzeri, F. Mauri, S. Piscanec, D. Jiang, K. S. Novoselov, S. Roth, A. K. Geim, *Phys. Rev. Lett.* **2006**, *97*, 187401.
- [55] Y. F. Hao, Y. Y. Wang, L. Wang, Z. H. Ni, Z. Q. Wang, R. Wang, C. K. Koo, Z. X. Shen, J. T. L. Thong, *Small* **2010**, *6*, 195.
- [56] K. Kim, S. Coh, L. Z. Tan, W. Regan, J. M. Yuk, E. Chatterjee, M. F. Crommie, M. L. Cohen, S. G. Louie, A. Zettl, *Phys. Rev. Lett.* **2012**, *108*, 246103.
- [57] H. M. Zhao, Y. C. Lin, C. H. Yeh, H. Tian, Y. C. Chen, D. Xie, Y. Yang, K. Suenaga, T. L. Ren, P. W. Chiu, *ACS Nano* **2014**, *8*, 10766.
- [58] R. R. Nair, P. Blake, A. N. Grigorenko, K. S. Novoselov, T. J. Booth, T. Stauber, N. M. R. Peres, A. K. Geim, *Science* **2008**, *320*, 1308.
- [59] X. S. Li, Y. W. Zhu, W. W. Cai, M. Borysiak, B. Y. Han, D. Chen, R. D. Piner, L. Colombo, R. S. Ruoff, *Nano Lett.* **2009**, *9*, 4359.
- [60] Y. Chen, J. Feng, F. X. Dong, Y. F. Li, Y. G. Bi, Y. Y. Yue, H. B. Sun, *Org. Electron.* **2016**, *38*, 35.